J. Korean Soc. Ind. Appl. Math. Vol.25, No.3, 66–81, 2021 https://doi.org/10.12941/jksiam.2021.25.066

REVIEW AND IMPLEMENTATION OF STAGGERED DG METHODS ON POLYGONAL MESHES

DOHYUN KIM[1], LINA ZHAO[2], AND EUN-JAE PARK[1,†]

[1]SCHOOL OF MATHEMATICS AND COMPUTING (COMPUTATIONAL SCIENCE AND ENGINEERING), YONSEI UNIVERSITY, SEOUL 03722, REPUBLIC OF KOREA
E-mail address: †ejpark@yonsei.ac.kr

[2]DEPARTMENT OF MATHEMATICS, CITY UNIVERSITY OF HONG KONG, HONG KONG SAR, CHINA

ABSTRACT. In this paper, we review the lowest order staggered discontinuous Galerkin methods on polygonal meshes in 2D. The proposed method offers many desirable features including easy implementation, geometrical flexibility, robustness with respect to mesh distortion and low degrees of freedom. Discrete function spaces for locally H^1 and $H(\mathrm{div})$ spaces are considered. We introduce special properties of a sub-mesh from a given star-shaped polygonal mesh which can be utilized in the construction of discrete spaces and implementation of the staggered discontinuous Galerkin method. For demonstration purposes, we consider the lowest case for the Poisson equation. We emphasize its efficient computational implementation using only geometrical properties of the underlying mesh.

1. INTRODUCTION

Traditional finite element methods are mostly developed for triangular or quadrilateral meshes. Recently, finite element methods making use of polygonal meshes received a lot of attention. Polygonal meshes are very flexible compared to traditional triangular and quadrilateral meshes. They can represent complex geometry accurately with relatively small number of elements. Also, allowing varying number of vertices for each element enables easy treatment of hanging nodes. This can be done by considering a hanging node as an additional vertex of a polygon. After the pioneering work of Wachspress [1], several numerical methods utilizing polygonal meshes are introduced. For example, virtual element methods ([2, 3]), hybrid high-order methods ([4, 5]), polygonal discontinuous Galerkin methods ([6, 7]), weak Galerkin methods ([8, 9]).

A staggered discontinuous Galerkin (DG) method is one of the polygonal finite element methods. The staggered DG method was first introduced by Chung and Engquist ([10]) to

Received August 6 2021; Revised September 20 2021; Accepted in revised form September 23 2021; Published online September 25 2021.

2000 *Mathematics Subject Classification.* 65N30.

Key words and phrases. Staggered grid, Discontinuous Galerkin method, Lowest order methods, Polygonal Meshes, Implementation, Static condensation.

† Corresponding author.

solve wave propagation problem on triangular meshes, which initiated a lot of works on solving problems arising from practical applications in the context of [11, 12, 13, 14, 15, 16, 17, 18, 19, 20, 21]. Recently, Zhao and Park [22] extended the horizon of staggered DG methods from triangular meshes to general polygonal meshes. Since then, staggered DG methods on polygonal meshes have been widely studied and applied to various physical problems arising from practical applications [23, 24, 25, 26, 27, 28, 29, 30]. The resulting method has many favorable features in the spirit of polygonal finite element methods while also preserving salient features of staggered DG methods; locally conservative; stable without stabilizing terms; superconvergence of primal variables; block-diagonal mass matrix. In contrast to other polygonal finite element methods, polygonal staggered DG methods are based on polynomial space on a triangular sub-mesh derived from the given polygonal mesh. Therefore, there is no need for local projection or construction of basis functions for the assembly of the discrete algebraic system. This allows very efficient computation based on well-developed implementation techniques for triangular finite element methods. Also, the global algebraic system size can be reduced by utilizing efficient static condensation due to block diagonal mass matrices and hybridized formulations [26, 31, 32, 33, 34, 35, 36, 37].

While staggered DG methods are well-established in the existing literatures, they are presented in abstract form. The purpose of this paper is to review the staggered DG method and highlight some computational aspects in more concrete form. For demonstrative purpose, we consider the simplest case: the lowest order staggered DG method for the Poisson model problem. The rest of this paper is organized as follows. In Section 2, notations for a polygonal mesh along with assumptions and its dual mesh will be introduced. Then locally conforming discrete spaces will be defined in Section 3. The Poisson equation will be considered in Section 4 with some implementation details. In Section 5, some numerical experiments are presented and some concluding remarks will be given in Section 6.

2. Polygonal Meshes and Staggered Meshes

In this section, we discuss the construction of a staggered mesh of a given polygonal mesh. The data structure of the staggered mesh will be provided with some implementation details.

Let $\Omega \subset \mathbb{R}^2$ be the domain of interest. For simplicity, we assume that Ω is a simple polygon. Let $\mathcal{P}_h$ be a polygonal mesh of Ω. We denote h_P by the diameter of a polygon $P \in \mathcal{P}_h$ and $\mathcal{P}_h$ satisfies

$$\overline{\Omega} = \bigcup_{P \in \mathcal{P}_h} \overline{P}, \quad h = \max_{P \in \mathcal{P}_h} h_P.$$

The following assumptions are often employed for the polygonal mesh:

Assumption (A): Every polygon P in $\mathcal{P}_h$ is composed of at most N_v vertices.
Assumption (B): Every polygon P in $\mathcal{P}_h$ is star-shaped with respect to a ball of radius $r \geq \rho_r h_P$, where ρ_r is a positive constant.
Assumption (C): For every polygon $P \in \mathcal{P}_h$ and every edge $e \in \partial P$, it satisfies $h_e \geq \rho_e h_P$, where ρ_e is a positive constant and h_e denotes the length of an edge e.

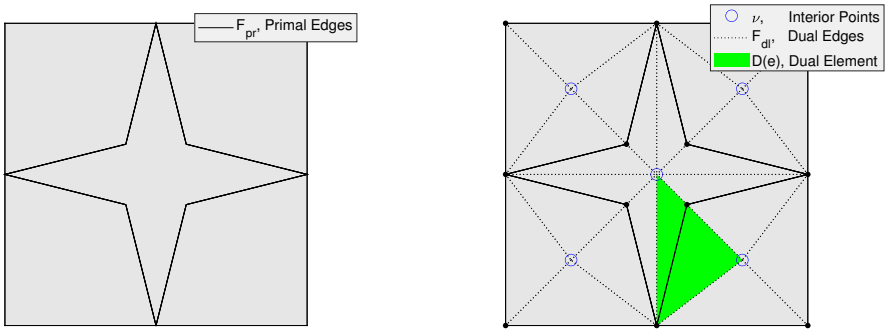

FIGURE 1. A given polygonal mesh $\mathcal{P}_h$ with five polygons (left) and its subdivision (right). A polygonal mesh is composed of four quadrilaterals and one concave octagon. In the right figure, each blue circle is an interior point ν of a primal element $P \in \mathcal{P}_h$, and dashed lines indicate dual edges. A dual element is highlighted in green.

Recent advances on polygonal finite element methods relaxes some assumptions so that more general polygonal meshes can be employed [30]. In this article, however, we assume that $\mathcal{P}_h$ satisfies the above three assumptions for simplicity of exposition.

In the following, we construct dual elements and dual edges from a sub-triangulation of $\mathcal{P}_h$. The following procedure is illustrated in Fig. 1. The triangular sub-mesh will be a building block of staggered DG methods. Let a polygon $P \in \mathcal{P}_h$ be given. The kernel $ker(P)$ is defined as the set of points in P visible from all vertices of P ($\mathcal{V}(P)$), i.e.,

$$ker(P) := \{\boldsymbol{x} \in P : \ (t\boldsymbol{x} + (1-t)\boldsymbol{v}) \in P, \ \forall \boldsymbol{v} \in \mathcal{V}(P), \ 0 < t < 1\}.$$

Assumption (B) ensures that $ker(P)$ has positive measure. By choosing an interior point $\nu \in ker(P)$, we obtain a non-degenerate triangulation of P by connecting ν and each vertex. This process induces a sub-triangulation $\mathcal{T}_h$ of $\mathcal{P}_h$. The set of all edges of $\mathcal{T}_h$ are denoted by $\mathcal{F}_h = \mathcal{F}_{pr} \dot{\cup} \mathcal{F}_{dl}$. The primal edges $\mathcal{F}_{pr}$ are all edges of $\mathcal{P}_h$, and dual edges $\mathcal{F}_{dl}$ are all additional edges obtained during the construction of $\mathcal{T}_h$. All dual edges are interior edges by construction, and we use $\mathcal{F}_{pr}^0$ and $\mathcal{F}_{pr}^b$ to represent interior and boundary primal edges, respectively. For each primal edge $e \in \mathcal{F}_{pr}$, we define a dual element $D(e)$ by the union of neighboring triangles of e and the set of all dual elements are denoted by $\mathcal{D}$. A dual element $D(e)$ is quadrilateral when $e \in \mathcal{F}_{pr}^0$ or triangular when $e \in \mathcal{F}_{pr}^b$.

Proposition 2.1. *Let $\mathcal{P}_h$ be a polygonal mesh and $\mathcal{T}_h$ be its sub-triangulation. Then the boundary of each triangle $T \in \mathcal{T}_h$ consists of one primal edge and two dual edges.*

Note that for a given $T \in \mathcal{T}_h$, there is one and only one edge $e \in \mathcal{F}_{pr}$ adjacent to T. In other words, there is exactly one dual element $D(e)$ containing T. This yields the following proposition.

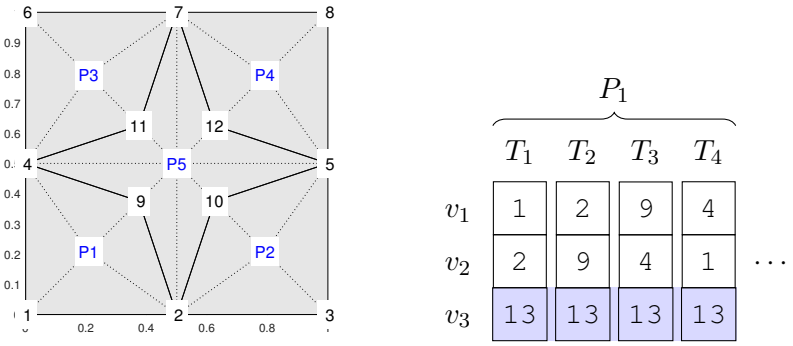

FIGURE 2. Global vertex numbering and element numbering (left) and data structure for sub-triangulation related to the first polygon P_1 (right). Note that the first two vertices of each triangle are a primal edge and the last vertex is the interior point of P_1. Also, $\overline{v_2v_3}$ and $\overline{v_3v_1}$ form dual edges, where the former pointing inward of the polygon and the latter pointing outward of the polygon.

Proposition 2.2. *The set of dual elements $\mathcal{D}$ forms a non-overlapping partition of Ω.*

Remark 2.3. *The above process can be extended to three-dimensional polyhedral mesh $\mathcal{P}_h$ where the boundary of polyhedron $P \in \mathcal{P}_h$ consists of, after subdivision of faces if necessary, triangular faces. Then we obtain a tetrahedral sub-mesh $\mathcal{T}_h$ and triangular faces $\mathcal{F}_h = \mathcal{F}_{pr} \dot{\cup} \mathcal{F}_{dl}$ by adjoining each vertex and an interior point. In this case, the boundary of a tetrahedron $T \in \mathcal{T}_h$ is one primal face and three dual faces.*

Let $e \in \mathcal{F}_{pr}^0 \cup \mathcal{F}_{dl}$ whose neighboring triangles are T^+ and T^-. Here, when $e \in \mathcal{F}_{dl}$, we assume that T^+ is always the "previous" triangle in counter-clockwise ordering of triangles within a polygon. We define a unique unit normal vector $\mathbf{n}_e$ and a unit tangential vector $\mathbf{t}_e$ of e by the outward unit normal vector and the counter-clockwise tangential vector of T^+ on e, respectively. Also, we write jump $[\![v]\!]_e = v|_{T^+} - v|_{T^-}$ and average $\{\!\{v\}\!\}_e = (v|_{T^+} + v|_{T^-})/2$ on an edge e. When $e \in \mathcal{F}_{pr}^b$ whose neighboring triangle is T, we set the unit normal vector and the tangential vector as the outward unit normal vector and the counter-clockwise tangential vector of Ω on e. The jump and average are defined as $[\![v]\!]_e = \{\!\{v\}\!\}_e = v|_T$. We omit e when there is no ambiguity.

In Remark 2.3, we can observe that the sub-triangulation has special properties. These properties are useful in the implementation with properly designed data structure. Figure 2 illustrates the data structure for the triangular mesh $\mathcal{T}_h$ for a general polygonal mesh.

3. Piecewise Conforming Discrete Spaces

In this section, we discuss piecewise conforming discrete spaces. We first define Sobolev spaces for scalar and vector variables:

$$H^1(\Omega) := \{v \in L^2(\Omega) : Dv \in L^2(\Omega)\},$$
$$H(\mathrm{div};\Omega) := \{\boldsymbol{\tau} \in [L^2(\Omega)]^2 : div(\boldsymbol{\tau}) \in L^2(\Omega)\},$$

where D and div are the weak derivative and divergence, respectively. When Ω is replaced by a set of open sets, we consider piecewise function space, e.g.,

$$H^1(\mathcal{T}_h) = \{v \in L^2(\Omega) : v|_T \in H^1(T)\ \forall T \in \mathcal{T}_h\}.$$

Let $\mathbb{P}_0(T)$ and $\mathbb{P}_0(e)$ be the constant function space on a triangle $T \in \mathcal{T}_h$ and an edge $e \in \mathcal{F}_h$, respectively. We denote $\mathbb{P}_0(\mathcal{O})$ as a piecewise constant function space when $\mathcal{O}$ is a set of open sets. In the remainder of this paper, C is a generic constant independent of h. The L^2-inner product and L^2-norm are denoted by $(\cdot,\cdot)_{\mathcal{O}}$ and $\|\cdot\|_{L^2(\mathcal{O})}$ for an open set $\mathcal{O} \subset \mathbb{R}^2$. When $\mathcal{O}$ is chosen as a collection of open sets we consider piecewise definition, e.g.,

$$(u,v)_{\mathcal{T}_h} = \sum_{T\in\mathcal{T}_h} (u,v)_T, \quad \|u\|_{L^2(\mathcal{T}_h)} = \left(\sum_{T\in\mathcal{T}_h} \|u\|^2_{L^2(T)}\right)^{1/2}.$$

To differentiate inner product on triangles and edges, we denote $\langle\cdot,\cdot\rangle_{\mathcal{F}_h}$ by L^2-inner product on edges. $\mathcal{T}_h$ or Ω will be omitted for L^2-inner product when there is no ambiguity.

Staggered DG methods are based on mixed formulations. Therefore, in general more than two carefully designed function spaces are considered for a problem. The discrete function spaces are chosen to be of equal-order, in general. As the name staggered DG suggests, the discrete function spaces are only locally conforming and their continuities are imposed on the staggered grid. In the remainder of this section, we consider the lowest order discrete spaces for staggered DG methods.

3.1. Piecewise H^1-space.

We define a piecewise H^1-space on each dual element $D(e)$. Since we are only considering the piecewise constant function space, this leads to the piecewise constant space on each dual element.

$$\begin{aligned} V_h &= \mathbb{P}_0(\mathcal{T}_h) \cap H^1(\mathcal{D}) \\ &= \{v \in \mathbb{P}_0(\mathcal{T}_h) : [\![v]\!] = 0\ \forall e \in \mathcal{F}^0_{pr}\} \\ &= \mathbb{P}_0(\mathcal{D}). \end{aligned}$$

We define the degrees of freedom for V_h by the average value on each primal edge

$$\phi(v) = \frac{1}{|e|}\int_e v\,\mathrm{d}s \quad \forall e \in \mathcal{F}_{pr}.$$

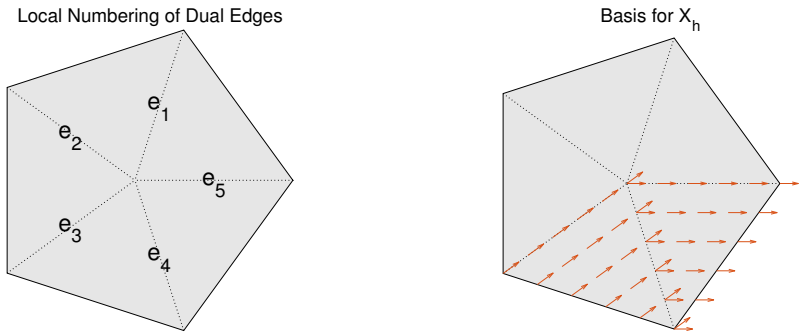

FIGURE 3. Local numbering of dual edges within a polygon (left) and the basis function $\boldsymbol{\tau}_{e_4}$ for X_h (right) defined in (3.1). Note that $\boldsymbol{\tau}_{e_4}$ is parallel to e_3 and e_5 so that $[\![\boldsymbol{\tau}_{e_4} \cdot \mathbf{n}]\!]_{e_3} = [\![\boldsymbol{\tau}_{e_4} \cdot \mathbf{n}]\!]_{e_5} = 0$. Also, we have $\boldsymbol{\tau}_{e_4} \cdot \mathbf{n} = 1$ on e_4 and hence it is continuous.

For given $e \in \mathcal{F}_{pr}$, the basis $\{v_e\}_{e\in\mathcal{F}_{pr}}$ of V_h can be defined by

$$v_e = \begin{cases} 1 & \text{in } \mathcal{D}(e), \\ 0 & \text{otherwise.} \end{cases}$$

By using the above degrees of freedom, we define an interpolation $I_h : H^1(\Omega) \to V_h$ by

$$\int_e (I_h v - v)\, \mathrm{d}s = 0 \quad \forall e \in \mathcal{F}_{pr}.$$

V_h is usually equipped with the mesh-dependent jump norm

$$\|v\|_{1,h}^2 = \sum_{e\in\mathcal{F}_{dl}} \frac{1}{h_e} \|[\![v]\!]\|_{L^2(e)}^2 .$$

3.2. **Piecewise $H(\mathrm{div})$-space.** For a piecewise $H(\mathrm{div})$-space, we consider a primal element-wise conforming space:

$$\begin{aligned} X_h &= [\mathbb{P}_0(\mathcal{T}_h)]^2 \cap H(\mathrm{div}; \mathcal{P}_h) \\ &= \{\boldsymbol{\tau} \in [\mathbb{P}_0(\mathcal{T}_h)]^2 : [\![\boldsymbol{\tau} \cdot \mathbf{n}]\!] = 0 \ \forall e \in \mathcal{F}_{dl}\}. \end{aligned}$$

Notice that the normal continuity is only imposed on dual edges. In other words, it allows discontinuity on primal edges in general. We define the degrees of freedom for X_h by the average normal value on each dual edge

$$\phi(\boldsymbol{\tau}) = \frac{1}{|e|} \int_e \boldsymbol{\tau} \cdot \mathbf{n}\, \mathrm{d}s \quad \forall e \in \mathcal{F}_{dl}.$$

Recall Proposition 2.1 that there are two dual edges for each triangle $T \in \mathcal{T}_h$. Therefore, we have two degrees of freedom for each triangle which coincide with the dimension of $[\mathbb{P}_0(T)]^2$.

For each $e \in \mathcal{F}_{dl}$, the basis $\{\boldsymbol{\tau}_e\}_{e\in\mathcal{F}_{dl}}$ of X_h can be defined by

$$\boldsymbol{\tau}_e = \begin{cases} \frac{1}{\mathbf{n}_e\cdot\mathbf{t}'}\mathbf{t}' & \text{in } T \in \mathcal{T}_h,\ e \in \partial T, \\ \mathbf{0} & \text{otherwise} \end{cases} \tag{3.1}$$

where $\mathbf{t}'$ is the tangential vector of the dual edge in ∂T other than e, see Fig. 3. The support of τ_e is only two triangles sharing a dual edge e. Again, we define an interpolation operator $J_h : H(\mathrm{div};\Omega) \to X_h$ by

$$\int_e (J_h\boldsymbol{\tau}\cdot\mathbf{n} - \boldsymbol{\tau}\cdot\mathbf{n})\,\mathrm{d}s = 0 \quad \forall e \in \mathcal{F}_{dl}.$$

X_h is equipped with the following norm

$$\|\boldsymbol{\tau}\|_{0,h}^2 = \|\boldsymbol{\tau}\|_{L^2(\Omega)}^2 + \sum_{e\in\mathcal{F}_{dl}} h_e \|\boldsymbol{\tau}\cdot\mathbf{n}\|_{L^2(e)}^2 .$$

The partial continuity of X_h and the special construction of $\mathcal{T}_h$ yield the following remarks.

Remark 3.1. *By the construction, the two neighbor triangles of a dual edge $e \in \mathcal{F}_{dl}$ are always contained in one polygon. This implies that the inner-product $(\boldsymbol{\tau}_e, \boldsymbol{\tau}_{e'})$ can be nonzero only when e and e' are contained in one polygon. Therefore, the mass matrix $M_{ij} = (\boldsymbol{\tau}_{e_i}, \boldsymbol{\tau}_{e_j})$ is block-diagonal. More specifically, $(\boldsymbol{\tau}_e, \boldsymbol{\tau}_{e'}) \neq 0$ only when e and e' are dual edges of a triangle. Then each of the block in M is a periodic tridiagonal matrix, see Fig. 4 for example.*

Furthermore, when square elements are considered, the mass matrix for X_h becomes a diagonal matrix, cf. Fig. 5. Indeed, when dual edges e and e' of a triangle are orthogonal, it holds $\boldsymbol{\tau}_e \cdot \boldsymbol{\tau}_{e'} = 0$ inside the triangle.

The following lemma is immediate from the Bramble-Hilbert lemma and the definition of interpolation operators.

Lemma 3.2. *The interpolation operators I_h, J_h are locally polynomial preserving operators and satisfies for $v \in H^1(T)$, $\boldsymbol{\tau} \in H^1(T)$, and $T \in \mathcal{T}_h$,*

$$\|I_h v - v\|_{L^2(T)} \le C h_T \|v\|_{H^1(T)},$$
$$\|J_h\boldsymbol{\tau} - \boldsymbol{\tau}\|_{L^2(T)} \le C h_T \|\boldsymbol{\tau}\|_{H^1(T)}.$$

Remark 3.3. *We use piecewise polynomial space on the triangulation $\mathcal{T}_h$. This allows us to consider efficient assembly procedure based on well-developed triangular finite element methods.*

Remark 3.4. *Discrete function spaces defined in this section can be extended to general polynomial degrees. Extension to three-dimensional space is straight-forward for the piecewise H^1-space and $H(\mathrm{div})$-space.*

4. POISSON EQUATION

Let $\Omega \subset \mathbb{R}^2$ be a simple polygonal domain. We seek a solution u satisfying

$$-\Delta u = f \text{ in } \Omega, \tag{4.1a}$$
$$u = g_D \text{ on } \Gamma_D, \tag{4.1b}$$
$$\partial_{\mathbf{n}} u = g_N \text{ on } \Gamma_N. \tag{4.1c}$$

Here, $\partial\Omega = \Gamma_D \dot{\cup} \Gamma_N$. The corresponding weak formulation is finding $u \in H^1(\Omega)$ with $u|_{\Gamma_D} = g_D$ such that

$$(\nabla u, \nabla v)_\Omega = (f, v)_\Omega + \langle g_N, v \rangle_{\Gamma_N} \quad \forall v \in H^1_{\Gamma_D}(\Omega).$$

Here, $H^1_{\Gamma_D}(\Omega) = \{v \in H^1(\Omega) : v|_{\Gamma_D} = 0\}$. Let a polygonal mesh $\mathcal{P}_h$ of Ω be given. We assume that for each $e \in \mathcal{F}^b_{pr}$, e is contained in only one of Γ_D or Γ_N.

4.1. **Discrete Formulation.** We introduce $\boldsymbol{\sigma} = \nabla u$ and multiply $\boldsymbol{\tau} \in X_h$ on both sides to obtain

$$\begin{aligned}(\boldsymbol{\sigma}, \boldsymbol{\tau}) &= (\nabla u, \boldsymbol{\tau}) \\ &= \sum_{T \in \mathcal{T}_h} \langle u, \boldsymbol{\tau} \cdot \mathbf{n}_T \rangle_{\partial T} \\ &= \langle u, [\![\boldsymbol{\tau} \cdot \mathbf{n}]\!] \rangle_{\mathcal{F}_h} \\ &= \langle u, [\![\boldsymbol{\tau} \cdot \mathbf{n}]\!] \rangle_{\mathcal{F}_{pr}} \\ &=: b^*_h(u, \boldsymbol{\tau}).\end{aligned}$$

Here, we utilized $u \in H^1(\Omega)$, $[\![\boldsymbol{\tau} \cdot \mathbf{n}]\!]_e = 0$ for $e \in \mathcal{F}_{dl}$, and $\mathbf{n}_T$ is outward unit normal vector of T. By the definition of $\boldsymbol{\sigma}$ and (4.1a), it holds for $v \in V^0_h$ that

$$\begin{aligned}(f, v) &= (-\nabla \cdot \boldsymbol{\sigma}, v) \\ &= -\sum_{T \in \mathcal{T}_h} \langle \boldsymbol{\sigma} \cdot \mathbf{n}_T, v \rangle_{\partial T} \\ &= -\langle \boldsymbol{\sigma} \cdot \mathbf{n}, [\![v]\!] \rangle_{\mathcal{F}_h} \\ &= -\langle \boldsymbol{\sigma} \cdot \mathbf{n}, [\![v]\!] \rangle_{\mathcal{F}_{dl}} - \langle g_N, v \rangle_{\Gamma_N} \\ &=: b_h(\boldsymbol{\sigma}, v) - \langle g_N, v \rangle_{\Gamma_N}.\end{aligned}$$

Finally, the discrete problem is to seek $(\boldsymbol{\sigma}_h, u_h) \in X_h \times V^{g_D}_h$ such that

$$(\boldsymbol{\sigma_h}, \boldsymbol{\tau}) - b^*_h(u_h, \boldsymbol{\tau}) = 0 \qquad \forall \boldsymbol{\tau} \in X_h, \tag{4.2a}$$
$$b_h(\boldsymbol{\sigma_h}, v) = (f, v) + \langle g_N, v \rangle_{\Gamma_N} \qquad \forall v \in V^0_h, \tag{4.2b}$$

where for $g \in L^2(\Gamma_D)$

$$V^g_h = \{v \in V_h : \int_e (v - g)\, \mathrm{d}s = 0 \ \forall e \in \mathcal{F}^b_{pr}, e \subset \Gamma_D\}.$$

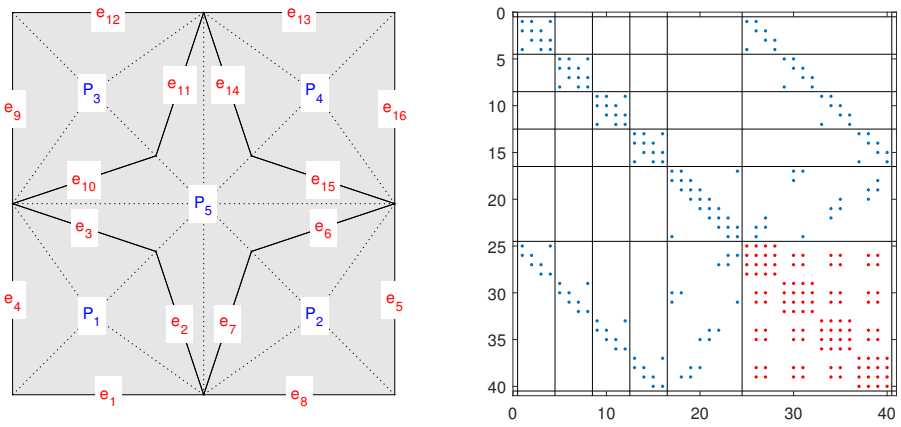

FIGURE 4. Left: A given polygonal mesh with polygon labels (blue) and primal edge labels (red). Right: Corresponding global (blue) and condensed (red) matrix structures. Observe that the mass matrix (left top corner of the matrix) is block-diagonal where each block is a symmetric periodic tridiagonal matrix.

Remark 4.1. *Since we are considering piecewise constant function spaces,* $B_{ij} = b_h(\boldsymbol{\tau}_{e_i}, v_{e_j})$ *can be represented using geometric quantities. Let* $T \in \mathcal{T}_h$ *be given and let* $e_i \in \mathcal{F}_{dl}$ *be the second edge and* $e_j \in \mathcal{F}_{pr}$ *be the first edge of* T*. Then we have*

$$\begin{aligned} b_h(\boldsymbol{\tau}_{e_i}, v_{e_j}) &= -\left\langle \boldsymbol{\tau}_{e_i} \cdot \mathbf{n}, [\![v_{e_j}]\!] \right\rangle_{e_i} \\ &= -|e_i|. \end{aligned}$$

Similarly, if $e_i \in \mathcal{F}_{dl}$ *is the third edge, we have*

$$b_h(\boldsymbol{\tau}_{e_i}, v_{e_j}) = |e_i|.$$

Lemma 4.2. *The discrete bilinear form* $b_h(\cdot,\cdot)$ *and* $b_h^*(\cdot,\cdot)$ *are adjoint*

$$b_h(\boldsymbol{\tau}, v) = b_h^*(v, \boldsymbol{\tau}) \quad \forall (\boldsymbol{\tau}, v) \in X_h \times V_h^0$$

so that the discrete problem is symmetric.

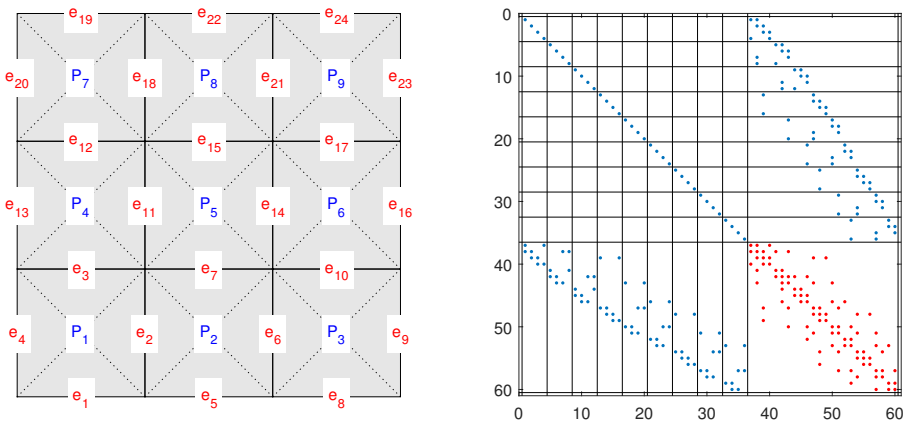

FIGURE 5. Left: A given square mesh with polygon labels (blue) and primal edge labels (red). Right: Corresponding global (blue) and condensed (red) matrix structures. Note that the mass matrix is diagonal and condensed matrix reduces to an edge-centered (dual-cell centered) finite volume method.

Proof. Recalling that v and $\boldsymbol{\tau}$ are piecewise constant functions, Green's theorem implies

$$\begin{aligned} b_h(\boldsymbol{\tau}, v) &= -\langle \boldsymbol{\tau}\cdot\mathbf{n}, [\![v]\!]\rangle_{\mathcal{F}_{dl}} \\ &= -\sum_{T\in\mathcal{T}_h}\int_{\partial T\cap\mathcal{F}_{dl}} (\boldsymbol{\tau}v)\cdot\mathbf{n}_T\,\mathrm{d}s \\ &= \sum_{T\in\mathcal{T}_h}\int_{\partial T\cap\mathcal{F}_{pr}} (\boldsymbol{\tau}v)\cdot\mathbf{n}_T\,\mathrm{d}s \\ &= \langle v, [\![\boldsymbol{\tau}\cdot\mathbf{n}]\!]\rangle_{\mathcal{F}_{pr}}. \end{aligned}$$

□

Remark 4.3. *Note that we have* $\langle v, [\![\boldsymbol{\tau}\cdot\mathbf{n}]\!]\rangle_e = 0$ *for* $e\subset\Gamma_D$ *and* $(v,\boldsymbol{\tau})\in V_h^0\times X_h$. *For simplicity, we do not remove these terms explicitly in this paper. In implementation, however, this should be under consideration.*

By using the basis functions of X_h and V_h and Lemma 4.2, we rewrite (4.2) as a matrix equation

$$\begin{bmatrix} M & B^t \\ B & 0 \end{bmatrix}\begin{bmatrix} \vec{\sigma} \\ \vec{u} \end{bmatrix} = \begin{bmatrix} 0 \\ F+G^N \end{bmatrix}$$

where $M_{ij}=(\boldsymbol{\tau}_{e_j},\boldsymbol{\tau}_{e_i})$, $B_{ij}=b_h(\boldsymbol{\tau}_{e_j},v_{e_i})$, $F_i=(f,v_{e_i})$, and $G_i^N=\langle g_N, v_{e_i}\rangle_{\Gamma_N}$.

Remark 4.4. *As discussed in Remark 3.1, the mass matrix in* (4.2) *is (block-)diagonal. Therefore, we can perform static condensation locally as in Algorithm 1. After static condensation,*

we obtain the Schur complement $S = BM^{-1}B^t$ for unknown u_h. Here, $S_{ij} \neq 0$ when e_i and e_j have a common neighboring polygon. Therefore, in the case of quadrilateral elements, the method reduces to a symmetric positive definite, edge-centered finite difference method for u_h with a stencil of 7 points, but only 5 points for square elements; see Fig. 5, cf. [38].

As we remove $\boldsymbol{\sigma}_h$ locally, dual edges can be constructed locally and need not be stored. This observation leads to the following algorithm.

Algorithm 1: Assembly of condensed matrix S.

Data: $\mathcal{P}_h$
Result: Condensed matrix S
Build $\mathcal{F}_{pr}$ from $\mathcal{P}_h$
$N \leftarrow$ the number of edges in $\mathcal{F}_{pr}$
Initialize $S \in \mathbb{R}^{N\times N}$
for $P \in \mathcal{P}_h$ **do**
  Place ν in $ker(P)$
  Connect each vertex of P and ν to create local sub-triangles $\mathcal{T}_P$
  $n \leftarrow$ the number of vertices of P
  Initialize $M^{loc}, B^{loc} \in \mathbb{R}^{n\times n}$ with zeros
  for $i \leftarrow 1$ **to** n **do**
    $A = area(T)$ where $T = conv(v_i, v_{i+1}, \nu)$
    Compute $\boldsymbol{\tau}_{e_1}$ and $\boldsymbol{\tau}_{e_2}$ related to T using (3.1)
    $M^{loc}_{(i:i+1,i:i+1)} \leftarrow M^{loc}_{(i:i+1,i:i+1)} + A \begin{bmatrix} \boldsymbol{\tau}_{e_1}\cdot\boldsymbol{\tau}_{e_1} & \boldsymbol{\tau}_{e_1}\cdot\boldsymbol{\tau}_{e_2} \\ \boldsymbol{\tau}_{e_1}\cdot\boldsymbol{\tau}_{e_2} & \boldsymbol{\tau}_{e_2}\cdot\boldsymbol{\tau}_{e_2} \end{bmatrix}$
    $B^{loc}_{i,i} \leftarrow -|\overline{v_2\nu}|$
    $B^{loc}_{i,i+1} \leftarrow |\overline{v_3\nu}|$
  end
  $J \leftarrow$global primal edge indices connected to P
  $S_{JJ} \leftarrow S_{JJ} + B^{loc}(M^{loc})^{-1}(B^{loc})^t$
end

Here, a periodic index is used for M^{loc} and B^{loc} for simplicity in Algorithm 1.

A polygonal mesh is composed of convex polygons in most cases, e.g., a bounded Voronoi diagram. In this case, ν can be chosen as the centroid of a polygon without computing $ker(P)$ as $ker(P) = P$ to reduce the computational cost.

4.2. **A Priori Error Estimates.** In this section, we discuss the well-posedness of the discrete problem and *a priori* error estimates. Thanks to the special construction of the staggered discrete spaces, staggered DG is stable without any additional stabilizing terms. This is beneficial as we do not have to fine tune the stability parameters which can be cumbersome in some applications. In the following, we have the discrete inf-sup condition [10, 22]:

Lemma 4.5. *There exists a positive constant C independent of h such that*

$$\inf_{v\in V_h}\sup_{\boldsymbol{\tau}\in X_h}\frac{b_h(\boldsymbol{\tau},v)}{\|\boldsymbol{\tau}\|_{0,h}\,\|v\|_{1,h}}\geq C.$$

The following theorem states the optimal convergence of discrete solutions assuming the full elliptic regularity. Also, superconvergence can be achieved. The superconvergence property is useful when we construct postprocessing.

Theorem 4.6. *Let $u\in H^1(\Omega)$ solve* (4.1) *and $u\in H^2(\Omega)$. If $\boldsymbol{\sigma}_h, u_h$ are the solution to* (4.2)*, then it holds*

$$\|\boldsymbol{\sigma}-\boldsymbol{\sigma}_h\|_{L^2(\Omega)}+\|u-u_h\|_{L^2(\Omega)}\leq Ch\,\|u\|_{H^2(\Omega)}\,.$$

Furthermore, we have

$$\|I_hu-u_h\|_{1,h}\leq Ch\,\|u\|_{H^2(\Omega)}\,.$$

It should be noted that if the problem allows low regularities, then one needs more sophisticated arguments; see, [22, 27], for further discussions.

5. Numerical Experiments

In this section, we investigate the convergence behavior of discrete solutions. Three different kinds of meshes are used: triangular; rectangular; polygonal meshes to demonstrate performance of staggered DG methods with various mesh configurations.

Consider the following problem with pure Dirichlet boundary condition:

$$\begin{aligned}-\Delta u&=2\pi^2\sin(\pi x)\sin(\pi y) && \text{in }\Omega,\\ u&=0 && \text{on }\partial\Omega\end{aligned}\tag{5.1}$$

where $\Omega=(0,1)^2$. Here, the solution is given by

$$u=\sin(\pi x)\sin(\pi y).$$

The convergence history is depicted in Fig. 7 on triangular, rectangular, and polygonal meshes, cf. Fig. 6. Convergence rates for $||u-u_h||_{L^2(\Omega)}$ and $||\boldsymbol{\sigma}-\boldsymbol{\sigma}_h||_{L^2(\Omega)}$ are 1 as expected. Also, $||I_hu-u_h||_{1,h}$ linearly converges as shown in Theorem 4.6 when triangular and polygonal meshes are used. However, we observe a quadratic convergence when rectangular meshes are used. We expect this behavior appears only when some special solutions are considered. Therefore, we consider another example with pure Dirichlet boundary condition:

$$u=\sin(x-y)\sin(x+y).\tag{5.2}$$

Data f and g_D can be derived from (4.1). Similarly to the previous case, convergence behavior is observed with three different mesh configurations, see Fig. 8. Now we have $\mathcal{O}(h)$ convergence for all three errors, $\|u-u_h\|_{L^2(\Omega)}$, $\|\boldsymbol{\sigma}-\boldsymbol{\sigma}_h\|_{L^2(\Omega)}$, and $\|I_hu-u_h\|_{1,h}$.

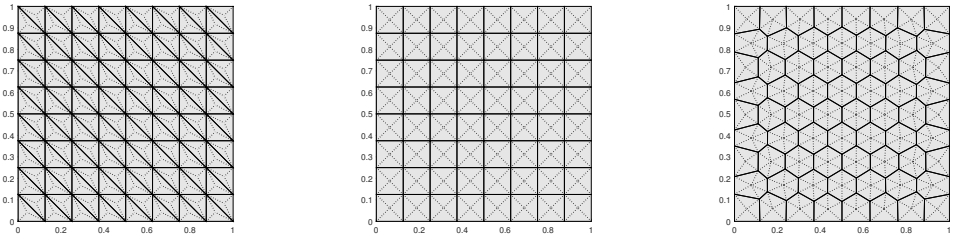

FIGURE 6. (Quasi-)Uniform meshes with $h \approx 2^{-3}$ used in the numerical experiment. From left to right, triangular, rectangular, and polygonal meshes.

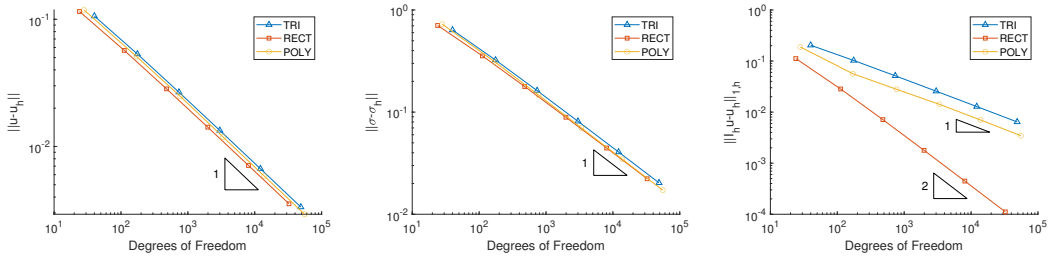

FIGURE 7. Convergence history for (5.1) with three different meshes. From left to right, $||u - u_h||_{L^2(\Omega)}$, $||\boldsymbol{\sigma} - \boldsymbol{\sigma}_h||_{L^2(\Omega)}$, and $||I_h u - u_h||_{1,h}$.

Lastly, we consider mixed boundary condition. We used the same solution of the previous example but with mixed boundary condition

$$\begin{aligned} u &= \sin(x-y)\sin(x+y) && \text{on } \Gamma_D, \\ \partial_{\mathbf{n}} u &= g_N && \text{on } \Gamma_N \end{aligned}$$

where $\Gamma_D = ((0,1) \times \{y = 1\}) \cup (\{x = 1\} \times (0,1))$ is the upper right boundary, Γ_N is the lower left boundary and g_N can be driven from the solution and the domain. Again, we observed similar convergence behavior as in the previous case, see Fig. 9.

6. CONCLUSION

In this paper, we reviewed staggered DG methods and presented some computational aspects of these methods. Construction of a simplicial sub-mesh from a polygonal mesh is introduced and special properties of the simplicial sub-mesh are investigated. Those properties are crucial for the construction of discrete spaces and efficient numerical experiments. Specific data structure for the sub-mesh is proposed to utilize these properties. Local static condensation of the flow variable is demonstrated which is embarrassingly parallelizable. We believe that this paper demonstrates staggered DG methods in more concrete way compared to existing works which are written in rather abstract forms.

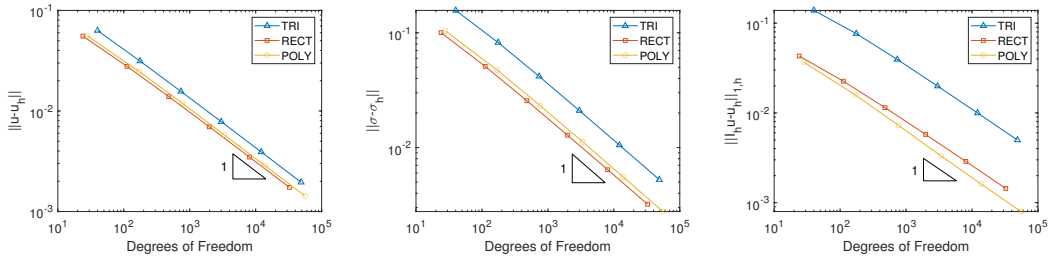

FIGURE 8. Convergence history for (5.2) with pure Dirichlet boundary condition. From left to right, $||u-u_h||_{L^2(\Omega)}$, $||\boldsymbol{\sigma}-\boldsymbol{\sigma}_h||_{L^2(\Omega)}$, and $||I_h u-u_h||_{1,h}$.

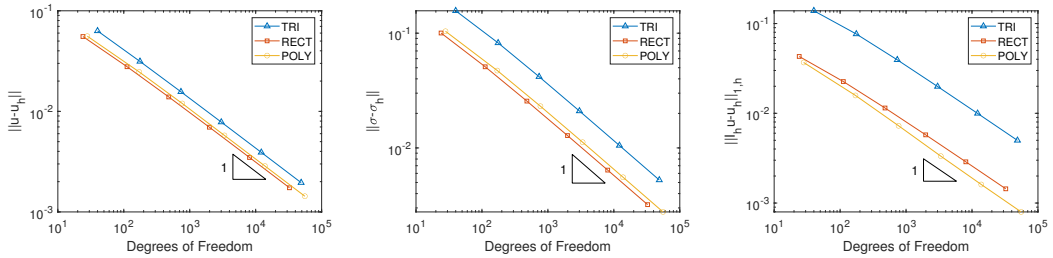

FIGURE 9. Convergence history for (5.2) with mixed boundary condition. From left to right, $||u-u_h||_{L^2(\Omega)}$, $||\boldsymbol{\sigma}-\boldsymbol{\sigma}_h||_{L^2(\Omega)}$, and $||I_h u-u_h||_{1,h}$.

ACKNOWLEDGMENT

The research of EJP was supported by the National Research Foundation of Korea (NRF) grant funded by the Ministry of Science and ICT
(NRF-2015R1A5A1009350 and NRF-2019R1A2C2090021).

REFERENCES

[1] E.L. Wachspress, *A Rational Finite Element Basis*, Academic Press, New York, New York, 1975.

[2] L. Beirão da Veiga, F. Brezzi, A. Cangiani, G. Manzini, L. D. Marini and A. Russo, *Basic principles of virtual element methods*, Mathematical Models and Methods in Applied Sciences, **23** (2013), 199–214.

[3] L. Beirão da Veiga, F. Brezzi, L. D. Marini and A. Russo *The Hitchhiker's Guide to the Virtual Element Method*, Mathematical Models and Methods in Applied Sciences, **24** (2014), 1541–1573.

[4] D. A. Di Pietro, A. Ern and S. Lemaire, *An arbitrary-order and compact-stencil discretization of diffusion on general meshes based on local reconstruction operators*, Computational Methods in Applied Mathematics, **14** (2014), 461-472.

[5] D. A. Di Pietro and J. Droniou, *The hybrid high-order method for polytopal meshes*, Springer International Publishing, 2020.

[6] F. Bassi, L. Botti, A. Colombo, D. A. Di Pietro and P. Tesini, *On the flexibility of agglomeration-based physical space discontinuous Galerkin discretizations*, Journal of Compututational Physics, **231** (2012), 45-65.

[7] P. F. Antonietti, S. Giani and P. Houston, *hp-version composite discontinuous Galerkin methods for elliptic problems on complicated domains*, SIAM Journal on Scientific Computing, **35** (2013), A1417A1439.

[8] J. Wang, and X. Ye, *A weak Galerkin finite element method for second-order elliptic problems*, Journal of Computational and Applied Mathematics, **241** (2013), 103–115.
[9] L. Mu, J. Wang and X. Ye, *Weak Galerkin finite element methods on polytopal meshes*, International Journal of Numerical Analysis and Modeling, **12** (2015), 31–53.
[10] E. T. Chung and B. Engquist *Optimal discontinuous Galerkin methods for wave propagation*, SIAM Journal on Numerical Analysis, **44** (2006), 2131–2158.
[11] E. T. Chung and B. Engquist *Optimal discontinuous Galerkin methods for the acoustic wave equation in higher dimensions*, SIAM Journal on Numerical Analysis, **47** (2009), 3820–3848.
[12] E. T. Chung and W. Qiu, *Analysis of an SDG method for the incompressible Navier-Stokes equations*, SIAM Journal on Numerical Analysis, **55** (2017), 543–569.
[13] E. T. Chung, P. Ciarlet Jr. and T. Yu, *Convergence and superconvergence of staggered discontinuous Galerkin methods for the three-dimensional Maxwells equations on Cartesian grids*, Journal on Computational Physics, **235** (2013), 14–31.
[14] E. T. Chung, H. H. Kim and O.B. Widlund, *Two-level overlapping Schwarz algorithms for a staggered discontinuous Galerkin method*, SIAM Journal on Numerical Analysis, **51** (2013), 47–67.
[15] H. H. Kim, E. T. Chung and C. S. Lee, *A staggered discontinuous Galerkin method for the Stokes system*, SIAM Journal on Numerical Analysis, **51** (2013), 3327–3350.
[16] E. T. Chung, C. Cockburn and G. Fu, *The staggered DG method is the limit of a hybridizable DG method*, SIAM Journal on Numerical Analysis, **52** (2014), 915–932.
[17] H. H. Kim, E. T. Chung and C.Y. Lam, *Mortar formulation for a class of staggered discontinuous Galerkin methods*, Computers & Mathematics with Applications, **71** (2016), 1568–1585.
[18] J.J. Lee and H. H. Kim, *Analysis of a staggered discontinuous Galerkin method for linear elasticity*, Journal of Scientific Computing, **66** (2016), 625–649.
[19] L. Zhao and E.-J. Park, *Fully computable bounds for a staggered discontinuous Galerkin method for the Stokes equations*, Computers & Mathematics with Applications, **75** (2018), 4115–4134.
[20] E. T. Chung, E.-J. Park and L. Zhao, *Guaranteed a posteriori error estimates for a staggered discontinuous Galerkin method*, Journal of Scientific Computing, **75** (2018), 1079–1101.
[21] L. Zhao and E.-J. Park, *A priori and a posteriori error analysis for a staggered discontinuous Galerkin method for convection dominant diffusion equations*, Journal of Computational and Applied Mathematics, **346** (2019), 63–83.
[22] L. Zhao and E.-J. Park, *A staggered discontinuous Galerkin method of minimal dimension on quadrilateral and polygonal meshes*, SIAM Journal on Scientific Computing, **40** (2018), A2543–A2567.
[23] L. Zhao, E.-J. Park and D.-w. Shin, *A staggered DG method of minimal dimension for the Stokes equations on general meshes*, Computer Methods in Applied Mechanics and Engineering, **345** (2019), 854–875.
[24] L. Zhao and E.-J. Park, *A lowest-order staggered DG method for the coupled Stokes-Darcy problem*, IMA Journal of Numerical Analysis, **40** (2020), 2871-2897.
[25] L. Zhao, E. T. Chung and M. Lam, *A new staggered DG method for the Brinkman problem robust in the Darcy and Stokes limits*, Computer Methods in Applied Mechanics and Engineering, **364** (2020), Paper No.112986, 13 pp.
[26] L. Zhao and E.-J. Park, *A new hybrid staggered discontinuous Galerkin method on general meshes*, Journal of Scientific Computing, **82** (2020), Paper No.12, 33 pp.
[27] L. Zhao and E.-J. Park, *A staggered cell-centered DG method for linear elasticity on polygonal meshes*, SIAM Journal on Scientific Computing, **42** (2020), A2158–A2181.
[28] L. Zhao, E.-J. Park and E. T. Chung, *Staggered discontinuous Galerkin methods for the Helmholtz equation with large wave number*, Computers & Mathematics with Applications, **80** (2020), 2676–2690.
[29] L. Zhao, E. T. Chung, E.-J. Park, and G. Zhou, Staggered DG Method for Coupling of the Stokes and Darcy–Forchheimer Problems, SIAM Journal on Numerical Analysis **59** (2021), 1–31.
[30] L. Zhao, D. Kim, E.-J. Park and E. Chung, *Staggered DG method with small edges for Darcy flows in fractured porous media*, https://arxiv.org/abs/2005.10955.

[31] D. Kim, L. Zhao and E.-J. Park, *Staggered DG methods for the pseudostress-velocity formulation of the Stokes equations on general meshes*, SIAM Journal on Scientific Computing, **42** (2020), A2537–A2560.
[32] Y. Jeon, E.-J. Park, *A hybrid discontinuous Galerkin method for elliptic problems*, SIAM J. Numer. Anal. 48 (5) (2010) 1968-1983.
[33] Y. Jeon, E.-J. Park, *New locally conservative finite element methods on a rectangular mesh*, Numerische Mathematik, 123 (2013), no.1, 97-119.
[34] Y. Jeon, E.-J. Park, D. Sheen, *A hybridized finite element method for the Stokes problem*, Computers & Mathematics with Applications Vol. 68, No. 12 Part B, (2014), 2222-2232.
[35] Y. Jeon, and E.-J. Park, D.-w. Shin, *Hybrid Spectral Difference Methods for an Elliptic Equation*, Comput. Methods Appl. Math. vol.17 no.2 (2017), 253-267.
[36] S. Yadav, A. Pani, and E.-J. Park, *Superconvergent discontinuous Galerkin methods for nonlinear elliptic equations*, Math. Comp. 82 (2013), no. 283, 1297–1335.
[37] M.-Y. KIM AND M. F. WHEELER, *A multiscale discontinuous galerkin method for convection–diffusion–reaction problems*, Computers & Mathematics with Applications, 68 (2014), pp. 2251–2261.
[38] T. Arbogast, C. N. Dawson, P. T. Keenan, M. F. Wheeler, and I. Yotov, *Enhanced cell-centered finite differences for elliptic equations on general geometry*, SIAM Journal on Scientific Computing, **19** (1998), 404–425.